

# Journal Pre-proof



Deep Learning-Based Nuclear Morphometry Reveals an Independent Prognostic Factor in Mantle Cell Lymphoma

Wen-Yu Chuang, Wei-Hsiang Yu, Yen-Chen Lee, Qun-Yi Zhang, Hung Chang, Lee-Yung Shih, Chi-Ju Yeh, Samuel Mu-Tse Lin, Shang-Hung Chang, Shir-Hwa Ueng, Tong-Hong Wang, Chuen Hsueh, Chang-Fu Kuo, Shih-Sung Chuang, Chao-Yuan Yeh

PII: S0002-9440(22)00282-6

DOI: <https://doi.org/10.1016/j.ajpath.2022.08.006>

Reference: AJPA 3786

To appear in: *The American Journal of Pathology*

Received Date: 10 May 2022

Revised Date: 18 July 2022

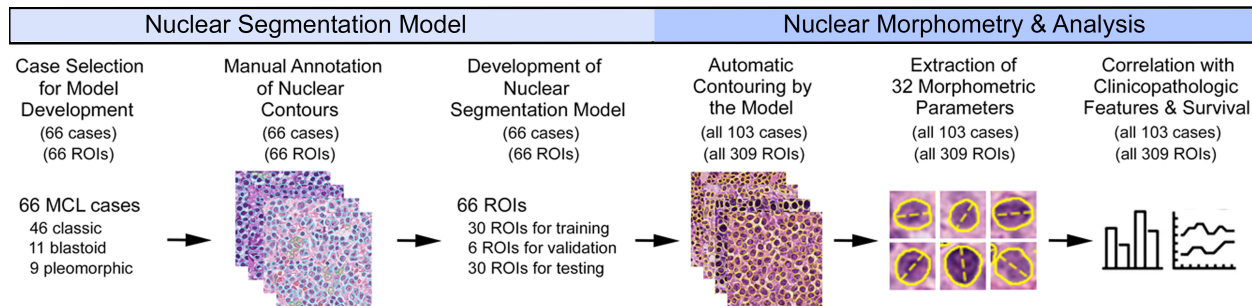
Accepted Date: 15 August 2022

Please cite this article as: Chuang W-Y, Yu W-H, Lee Y-C, Zhang Q-Y, Chang H, Shih L-Y, Yeh C-J, Mu-Tse Lin S, Chang S-H, Ueng S-H, Wang T-H, Hsueh C, Kuo C-F, Chuang S-S, Yeh C-Y, Deep Learning-Based Nuclear Morphometry Reveals an Independent Prognostic Factor in Mantle Cell Lymphoma, *The American Journal of Pathology* (2022), doi: <https://doi.org/10.1016/j.ajpath.2022.08.006>.

This is a PDF file of an article that has undergone enhancements after acceptance, such as the addition of a cover page and metadata, and formatting for readability, but it is not yet the definitive version of record. This version will undergo additional copyediting, typesetting and review before it is published in its final form, but we are providing this version to give early visibility of the article. Please note that, during the production process, errors may be discovered which could affect the content, and all legal disclaimers that apply to the journal pertain.

Copyright © 2022 Published by Elsevier Inc. on behalf of the American Society for Investigative Pathology.

## Deep Learning-Based Nuclear Morphometry in Mantle Cell Lymphoma



Conclusion: A morphometric score calculated from the skewness and mean of nuclear irregularity ( $P = 0.0038$ ) was an independent prognostic factor in addition to bMIPI risk group ( $P = 0.025$ ), and a summed morphometric bMIPI score was useful for risk stratification of MCL patients ( $P = 0.000001$ ).

1   **Deep Learning-Based Nuclear Morphometry Reveals**  
2   **an Independent Prognostic Factor in Mantle Cell**  
3   **Lymphoma**

4

5   Wen-Yu Chuang,<sup>\*†‡§</sup> Wei-Hsiang Yu,<sup>¶</sup> Yen-Chen Lee,<sup>†</sup> Qun-Yi Zhang,<sup>¶</sup> Hung  
6   Chang,<sup>†||</sup> Lee-Yung Shih,<sup>†||</sup> Chi-Ju Yeh,<sup>\*†</sup> Samuel Mu-Tse Lin,<sup>¶\*\*</sup> Shang-Hung  
7   Chang,<sup>†††</sup> Shir-Hwa Ueng,<sup>\*†‡</sup> Tong-Hong Wang,<sup>‡‡</sup> Chuen Hsueh,<sup>\*†‡</sup> Chang-Fu  
8   Kuo,<sup>†§§</sup> Shih-Sung Chuang,<sup>¶¶</sup> and Chao-Yuan Yeh<sup>¶</sup>

9

10   *From the Department of Pathology,\* Chang Gung Memorial Hospital and*  
11   *Chang Gung University; the School of Medicine<sup>†</sup> and the Chang Gung*  
12   *Molecular Medicine Research Center,<sup>‡</sup> Chang Gung University; the Center for*  
13   *Vascularized Composite Allotransplantation,<sup>§</sup> the Division of Hematology and*  
14   *Oncology,<sup>||</sup> Department of Internal Medicine, the Center for Big Data Analytics*  
15   *and Statistics,<sup>††</sup> the Tissue Bank,<sup>‡‡</sup> and the Center for Artificial Intelligence in*  
16   *Medicine,<sup>§§</sup> Chang Gung Memorial Hospital, Taoyuan; the Taipei American*  
17   *School,\*\* the aetherAI, Co., Ltd.,<sup>¶</sup> Taipei; and the Department of Pathology,<sup>¶¶</sup>*  
18   *Chi-Mei Medical Center, Tainan, Taiwan*

19

20 Number of text pages: 59

21 Number of tables: 7

22 Number of figures: 4

23

24 Short running head: Deep Learning-Based Morphometry in MCL

25

26 Funding: This study was partly supported by grants from Ministry of Science

27 and Technology, Taiwan (MOST109-2314-B-182-063; to W.-Y. C.), Chang

28 Gung Medical Foundation (CIRPG3H0011 and CMRPG3K0701; to W.-Y. C.),

29 and Johnson & Johnson Taiwan Ltd. (T19016; to S.-S. C.).

30

31 Address correspondence to (1) Chao-Yuan Yeh, MD, aetherAI Co., Ltd., Rm.

32 907, 9F, No. 3-2, Yuanqu Street, Nangang District, Taipei City 115603, Taiwan.

33 E-mail: joeyeh@aetherai.com and (2) Shih-Sung Chuang, MD, Department of

34 Pathology, Chi-Mei Medical Center, No. 901, Chunghwa Road, Yongkang

35 District, Tainan City 710402, Taiwan. E-mail: cmh5301@mail.chimei.org.tw

36

37 Conflicts of interest: Chao-Yuan Yeh is the Chief Executive Officer and a co-

38 founder of aetherAI. Wei-Hsiang Yu is a data scientist of aetherAI. Qun-Yi

39 Zhang and Samuel Mu-Tse Lin are research assistants of aetherAI. The  
40 authors have no other conflicts of interest to declare.

41 **Abstract**

42 Blastoid/pleomorphic morphology is associated with short survival in mantle  
43 cell lymphoma (MCL), but its prognostic value is overridden by proliferation  
44 index Ki-67 in multivariate analysis. Here we developed a nuclear  
45 segmentation model using deep learning, and nuclei of tumor cells in 103  
46 MCL cases were automatically delineated. Eight nuclear morphometric  
47 attributes, including length, width, perimeter, area, length/width ratio,  
48 circularity, irregularity, and entropy, were extracted from each nucleus. The  
49 mean, variance, skewness, and kurtosis of each attribute were calculated for  
50 each case, resulting in 32 morphometric parameters. Compared to classic  
51 MCL, 17 morphometric parameters were significantly different in  
52 blastoid/pleomorphic MCL. Using univariate analysis, 16 morphometric  
53 parameters (including 14 significantly different between classic and  
54 blastoid/pleomorphic MCL) were significant prognostic factors. Using  
55 multivariate analysis, biologic MCL international prognostic index (bMIPI) risk  
56 group ( $P=0.025$ ), low skewness of nuclear irregularity ( $P=0.020$ ), and high  
57 mean of nuclear irregularity ( $P=0.047$ ) were independent adverse prognostic  
58 factors. Furthermore, a morphometric score calculated from the skewness  
59 and mean of nuclear irregularity ( $P=0.0038$ ) was an independent prognostic

60 factor in addition to bMIPI risk group ( $P=0.025$ ), and a summed morphometric  
61 bMIPI score was useful for risk stratification of MCL patients ( $P=0.000001$ ).  
62 Our results demonstrate for the first time that a nuclear morphometric score is  
63 an independent prognostic factor in MCL. It is more robust than  
64 blastoid/pleomorphic morphology and can be objectively measured.

65 **Introduction**

66 Mantle cell lymphoma (MCL) is a rare type of B-cell lymphoma with a largely  
67 aggressive clinical course.<sup>1</sup> Most MCL cases have a *CCND1* translocation  
68 resulting in overexpression of cyclin D1 and subsequent dysregulation of cell  
69 cycle. Occasionally, MCL could lack the *CCND1* translocation and cyclin D1  
70 overexpression, but it still shares similar clinical features and gene expression  
71 profiles with cyclin D1-positive MCL.<sup>2,3</sup> Such cyclin D1-negative MCL can be  
72 identified with SOX11 positivity.<sup>4-7</sup> Most MCL patients present with an  
73 advanced stage III or IV disease with lymphadenopathy, hepatosplenomegaly,  
74 and bone marrow involvement.<sup>1</sup> The median survival of MCL patients is about  
75 3 to 5 years.<sup>1</sup> Identification of patients with poor prognosis would be helpful,  
76 since more aggressive treatment, such as hematopoietic stem cell transplant,  
77 could be considered for these patients. Mantle Cell Lymphoma International  
78 Prognostic Index (MIPI), which includes patient age, Eastern Cooperative  
79 Oncology Group (ECOG) performance score, serum lactate dehydrogenase  
80 (LDH) level, and white blood cell count, is an important clinical prognostic  
81 factor for MCL patients with an advanced disease.<sup>8</sup> High proliferation rate is  
82 also associated with poor prognosis in MCL.<sup>1</sup> Biologic MIPI (bMIPI), which  
83 combines MIPI and the proliferation index Ki-67, has even stronger prognostic

84 value than MIPI.<sup>8</sup> Unlike most MCL patients with extensive nodal involvement,  
85 a small subset of MCL cases present as leukemic non-nodal MCL, which  
86 usually follows an indolent clinical course.<sup>9</sup>

87 MCL is usually composed of monomorphic small to medium-sized  
88 lymphoid cells with irregular nuclei (classic MCL).<sup>1</sup> A minor subgroup of MCL  
89 cases is composed of larger lymphoid cells with blastoid or pleomorphic nuclei  
90 (blastoid or pleomorphic variant), and these tumors have an even more  
91 aggressive biologic behavior.<sup>1</sup> Blastoid MCL is composed of medium-sized  
92 lymphoid cells with fine chromatin and small nucleoli, morphologically similar  
93 to lymphoblasts. Pleomorphic MCL is composed of medium-sized to large  
94 lymphoid cells with pleomorphic nuclei and more prominent nucleoli. Although  
95 blastoid/pleomorphic morphology is associated with poor prognosis, it has  
96 been shown that the prognostic value was overridden by proliferation index  
97 Ki-67 in multivariate analysis.<sup>10</sup> Despite the apparent correlation between  
98 morphology and prognosis, the prognostic significance of morphometric  
99 parameters in MCL has not been evaluated to date.

100 In this study, we developed a deep learning algorithm to automatically  
101 delineate nuclear contours of MCL tumor cells. Morphometric parameters  
102 were extracted and calculated, and their prognostic significance was

103 evaluated.

104

105 **Materials and Methods**

106 **Case Selection**

107 The overview of the study design is shown in Figure 1. A total of 103 MCL  
108 cases diagnosed between 2002 and 2019 were retrieved from the archives of  
109 Departments of Pathology of two medical centers in Taiwan (Chang Gung  
110 Memorial Hospital at Taoyuan and Chi-Mei Medical Center at Tainan). The  
111 pathology slides were reviewed by two senior hematopathologists (W.-Y.  
112 Chuang and S.-S. Chuang) to confirm the diagnosis. Cases with less than  
113 three high-quality regions were excluded. A high-quality region was defined as  
114 a square of 0.25 x 0.25 mm, in which more than 95% of the nucleated cells  
115 were tumor cells and no prominent artifacts such as crushing, tissue folding,  
116 areas out of focus, or air bubbles were found. For difficult cases,  
117 immunostained slides were used to identify areas with a high tumor cell  
118 percentage. All specimens of biopsy or resection from either lymph nodes or  
119 extranodal sites were obtained before treatment. All cyclin D1-negative cases  
120 were positive for SOX11 (clone MRQ-58).<sup>4-7</sup> Cases of leukemic non-nodal  
121 MCL were excluded due to their unique indolent clinical behavior.<sup>9</sup> All cases

122 were restaged according to the Lugano classification.<sup>11</sup> For each case, one  
123 routine 3-μm-thick section of formalin-fixed paraffin embedded tissue with  
124 hematoxylin and eosin stain was used for digitization. Whole-slide high-  
125 resolution digital images were produced using a NanoZoomer S360 digital  
126 slide scanner (Hamamatsu Photonics, Hamamatsu, Japan) with a 40×  
127 objective mode. Three high-quality regions per slide were selected by a senior  
128 hematopathologist (W.-Y. Chuang). This study had been approved by the  
129 Institutional Review Board of Chang Gung Medical Foundation (IRB No.  
130 201902130B0 and 202000483B0).

131

### 132 Computer Hardware and Software

133 We conducted our experiments on a customized server with an NVIDIA  
134 QUADRO RTX 8000 graphics processing unit (GPU). The instance detection  
135 module and feature extracting algorithms were implemented with Python 3.7  
136 and PyTorch 1.7 on a Linux platform. The statistical analyses were performed  
137 using the IBM SPSS Statistics 20.0 and R language on a Windows platform.

138

### 139 Nuclear Detection Model

140 Among the 309 selected high-quality regions, 66 regions of interest (ROIs)

141 with a size of 132 x 132  $\mu\text{m}$  were randomly sampled from 66 different cases  
142 for training (30 cases), validation (6 cases), and testing (30 cases) of the  
143 nuclear detection model. The case numbers of different morphologic subtypes  
144 were balanced in each data set (Table 1). All nuclear contours of tumor cells in  
145 the 66 ROIs (10459 nuclei) were manually annotated under the supervision of  
146 a senior hematopathologist (W.-Y. Chuang) using a free-hand contouring tool  
147 on aetherSlide Digital Pathology System (aetherAI, Taipei, Taiwan). For the  
148 testing set, all nuclear contours of non-tumor cells in the 30 ROIs (347 nuclei)  
149 were manually annotated by a senior hematopathologist (W.-Y. Chuang). The  
150 numbers of cases, ROIs, and annotated cells of each morphologic variant in  
151 each data set are shown in Table 1.

152 A two-stage instance segmentation model was employed to detect nuclei  
153 in the images. Our model was implemented using MMDetection,<sup>12</sup> an open-  
154 source software for object detection and instance segmentation, and trained  
155 with COCO<sup>13</sup> formatted cell annotations. To be specific, a hybrid task cascade  
156 region proposal convolutional neural network, or HTC-RCNN,<sup>14</sup> with a  
157 ResNet50<sup>15</sup> backbone was trained to segment the nuclear contour of each  
158 tumor cell in an image. Images were randomly augmented on-the-fly during  
159 the training phase to increase the data variability. The applied data

160 augmentation methods included random translation, random scaling, random  
161 rotation, random horizontal/vertical flipping, random color jittering, and random  
162 Gaussian blurring. The increased diversity of training images is known to  
163 make the model more generalizable and robust.<sup>16</sup> The model was trained with  
164 a stochastic gradient descent optimizer, a learning rate of 0.001, and a batch  
165 size of 16 for 1200 epochs. Non-maximum suppression technique was  
166 employed to remove overlapping nuclei of model predictions. It selected one  
167 out of multiple overlapping instances which have an intersection over union  
168 ( $\text{IoU}$ )  $\geq 0.5$  by keeping the most confident instance.

169 The performance of the nuclear detection model was evaluated by mean  
170 average precision. In brief, an IoU was calculated for each predicted bounding  
171 box to assess the extent of overlapping with a ground truth bounding box. A  
172 prediction was considered correct if the IoU was at least 0.5. The precision  
173 and recall of nuclear prediction were calculated from the highest prediction  
174 score object to the lowest one ranging from 1 to 0 iteratively. The average  
175 precision of each object class was then calculated by summing up the area  
176 under the precision-recall curve. Finally, the mean average precision can be  
177 derived by averaging the average precision of different object classes. Since  
178 we segmented only one object class, namely tumor cell nucleus, the mean

179 average precision is the same as the average precision. A bootstrapping  
180 method was employed to estimate the 95% confidence interval (95% CI) of  
181 mean average precision. In brief, the dataset was resampled through a  
182 sampling-with-replacement manner followed by evaluating the mean average  
183 precision for 1000 times. The lower bound and the upper bound of the target  
184 statistics were computationally derived by taking the 2.5 and 97.5 percentile of  
185 the distribution, respectively. Mean IoU, mean Sørensen-Dice coefficient, and  
186 average aggregated Jaccard index were calculated to evaluate the similarity  
187 between segmented nuclei and annotated nuclei.

188

#### 189 Feature Extraction Procedure

190 For each case, an ROI of  $132 \times 132 \mu\text{m}$  was randomly cropped from each  
191 high-quality region. The three ROIs of each case were analyzed by our  
192 nuclear detection model, and eight nuclear morphometric attributes related to  
193 nuclear size (length, width, perimeter, and area), shape (length/width ratio,  
194 circularity, and irregularity), and texture (entropy) were extracted from each  
195 detected nucleus. The definition of each morphometric attribute is listed  
196 below:

197 1. Nuclear length: length of the longest axis of the nucleus.

198     2. Width: length of the axis orthogonal to the longest axis of the nucleus.

199     3. Perimeter: length of the nuclear boundary.

200     4. Area: area within the nuclear boundary.

201     5. Length/width ratio: ratio of the nuclear length to the nuclear width.

202     6. Circularity: ratio of the nuclear area to the area of a circle with a diameter  
203                 of the nuclear length.

204     7. Irregularity: variance of the distance from the nuclear center to vertices of  
205                 the nuclear boundary.

206     8. Entropy: randomness of the intensity of pixels within the nuclear boundary.

207         The four statistical moments, including mean, variance, skewness, and  
208         kurtosis, of each attribute were calculated across all three ROIs for each case,  
209         resulting in a total of 32 morphometric parameters. The statistical moments  
210         are used to describe different characteristics of the probability density function  
211         of a random variable. The first moment, or mean, is the expected value of a  
212         random variable. The second moment, or variance, is the expected squared  
213         difference of a random variable from its mean. The third moment, or  
214         skewness, is a measure of the asymmetry of the probability distribution. The  
215         fourth moment, or kurtosis, is a measure of the heaviness of tails of the  
216         probability distribution.

217

218 Statistical Analysis

219 Differences between categorical data were assessed by chi-square test, and

220 Yates' correction was performed when the expected frequency was less than

221 5. Continuous parameters were compared using Student's t-test. The cutoff

222 value of each morphometric parameter with the highest survival influence was

223 determined by a free R-based software Evaluate Cutpoints<sup>17</sup> (available at

224 <http://wnbikp.umed.lodz.pl/Evaluate-Cutpoints/>, last accessed Jul 17, 2022)

225 using the 'cutp' algorithm. In brief, a Cox proportional hazards model was

226 used to calculate the influence of a parameter on survival. An optimal cutoff

227 value was then determined statistically by a log-rank test through comparing

228 the test statistic to a Brownian bridge distribution. A value larger than the

229 cutoff value was considered high. Overall survival was analyzed by the

230 Kaplan-Meier method and compared by log-rank tests. The influence of

231 parameters on overall survival was analyzed using univariate or multivariate

232 Cox regression. A *P*-value less than 0.05 was considered statistically

233 significant. To further examine the robustness of each morphometric

234 parameter on prognostic effect, a bootstrapping was performed with the

235 number of repetitions set to 1000.

236

237 **Results**

238 **Clinicopathologic Features**

239 The clinicopathologic features of our MCL cases and their influence on overall

240 survival are listed in Table 2. The age at diagnosis ranged from 33 to 96

241 years, with a median of 64. There was prominent male predominance

242 (83.5%), and 88.8% of cases had an advanced stage III or IV disease. The

243 induction therapy used included CHOP (cyclophosphamide, doxorubicin,

244 vincristine, and prednisolone) (n = 19), R (rituximab)-CHOP (n = 16), COP

245 (cyclophosphamide, vincristine, and prednisolone) (n = 13), R-COP (n = 7),

246 VR-CAP (bortezomib, rituximab, cyclophosphamide, doxorubicin, and

247 prednisolone) (n = 7), hyper-CVAD (cyclophosphamide, vincristine,

248 doxorubicin, and dexamethasone) (n = 4), R-hyper-CVAD (n = 4), BR

249 (bendamustine and rituximab) (n = 2), CEOP (cyclophosphamide, epirubicin,

250 vincristine, and prednisolone) (n = 2), R-CEOP (n = 2), and other regimens (n

251 = 7). Ten patients were not eligible for treatment, and the information of

252 treatment were not available for other ten patients. Using univariate analysis,

253 age greater than 60 years at diagnosis ( $P = 0.0026$ ), stage III or IV disease ( $P$

254 = 0.018), presence of B symptoms ( $P = 0.011$ ), elevated serum LDH level ( $P =$

255 0.0079), ECOG score more than 1 ( $P = 0.030$ ), blastoid/pleomorphic  
256 morphology ( $P = 0.0085$ ), and proliferation index Ki-67  $\geq 30\%$  ( $P = 0.0070$ )  
257 were significant adverse prognostic factors. In addition, bMIPI risk group had  
258 stronger influence on overall survival ( $P = 0.000099$ ) compared to MIPI risk  
259 group ( $P = 0.00037$ ). The survival curves of patients stratified by  
260 clinicopathologic features with significant prognostic value are shown in  
261 Figure 2A-I.

262

## 263 Nuclear Detection and Feature Extraction

264 The learning curves and precision-recall curves of our nuclear detection  
265 model are shown in Figure 3A and Figure 3B, respectively. The mean average  
266 precision was 0.887 (95% CI: 0.845–0.892) and 0.836 (95% CI: 0.832–0.840)  
267 for the validation and testing set, respectively. Our algorithm achieved a  
268 precision of 0.909 (95% CI: 0.891–0.924) with a recall of 0.835 (95% CI:  
269 0.817–0.857) in the testing set. Regarding different morphologic variants, the  
270 mean average precision was 0.837 (95% CI: 0.825–0.860), 0.875 (95% CI:  
271 0.829–0.929), and 0.799 (95% CI: 0.736–0.844) for classic, blastoid, and  
272 pleomorphic MCL, respectively (Figure 3C). The mean IoU was 0.686, 0.680,  
273 and 0.680 for classic, blastoid, and pleomorphic MCL, respectively. The mean

274 Sørensen-Dice coefficient was 0.813, 0.801, and 0.810 for classic, blastoid,  
275 and pleomorphic MCL, respectively. The average aggregated Jaccard index of  
276 predicted nuclei was 0.696, 0.696, and 0.685 for classic, blastoid, and  
277 pleomorphic MCL, respectively. Examples of automatic nuclear detection and  
278 contouring (yellow closed lines) of MCL cases with classic, blastoid, and  
279 pleomorphic morphology are demonstrated in Figure 3D. Among all predicted  
280 nuclei in the testing set, the mean proportion of non-tumor cell nuclei was  
281 0.85% (0.93% in classic MCL; 0.89% in blastoid MCL; 0.38% in pleomorphic  
282 MCL). The nuclear segmentation results of representative ROIs of all cases  
283 can be found in Supplemental Figure S1. The mean nuclear length, width,  
284 perimeter, area, length/width ratio, circularity, irregularity, and entropy of all  
285 cases were  $8.440 \pm 0.898 \mu\text{m}$  (mean  $\pm$  standard deviation),  $6.587 \pm 0.710 \mu\text{m}$ ,  
286  $24.900 \pm 2.677 \mu\text{m}$ ,  $45.125 \pm 9.739 \mu\text{m}^2$ ,  $1.293 \pm 0.032$ ,  $0.759 \pm 0.015$ ,  $0.173$   
287  $\pm 0.044 \mu\text{m}^2$ , and  $5.752 \pm 0.228$ , respectively.

288

289 Comparison of Morphometric Parameters between Morphologic

290 Variants

291 Comparison of the 32 morphologic features between classic MCL and blastoid  
292 or pleomorphic MCL is shown in Table 3. Compared to classic MCL, 17

293 morphometric parameters were significantly different in blastoid/pleomorphic  
294 MCL. These different parameters were related to nuclear size (length, width,  
295 perimeter, and area) and shape (irregularity), and blastoid or pleomorphic  
296 MCL had higher mean, higher variance, lower skewness, and/or lower  
297 kurtosis compared to classic MCL. We demonstrated that the aggressive  
298 morphologic variants diagnosed by hematopathologists truly had different  
299 objective morphometric features.

300

301 **Correlation of Morphometric Parameters with Overall Survival**  
302 Using univariate analysis, the influence of nuclear morphometric parameters  
303 on overall survival is listed in Table 4. Sixteen of the 32 morphometric  
304 parameters (including 14 significantly different between classic and  
305 blastoid/pleomorphic MCL) had significant influence on survival. Of note, all  
306 16 morphometric parameters remained significant prognostic factors after  
307 bootstrapping for 1000 times, confirming the robustness of prognostic effect.  
308 These morphometric parameters with prognostic significance were related to  
309 nuclear size (length, width, perimeter, and area) and shape (length/width ratio  
310 and irregularity), and short survival was correlated with higher mean, higher  
311 variance, lower skewness, and/or lower kurtosis. The distribution of each

312 nuclear morphometric parameter with a cutoff value determined by the  
313 software Evaluate Cutpoints<sup>17</sup> and the survival curves stratified by each  
314 morphometric parameter using the cutoff value are shown in Supplemental  
315 Figure S2.

316

317 Multivariate Analysis of Parameters for Overall Survival  
318 The results of multivariate analysis of morphometric parameters and  
319 independent clinicopathologic parameters for overall survival are listed in  
320 Table 5. Among the 16 morphometric parameters with significant influence on  
321 overall survival in univariate analysis, only low skewness of nuclear  
322 irregularity ( $P = 0.0054$ ) and high mean of nuclear irregularity ( $P = 0.033$ )  
323 remained significant adverse prognostic factors. Among the seven  
324 independent clinicopathologic parameters with significant adverse prognostic  
325 influence in univariate analysis, only age greater than 60 years at diagnosis  
326 remained significant ( $P = 0.025$ ). Of note, blastoid/pleomorphic morphology  
327 and Ki-67 $\geq 30\%$  were no more significant in multivariate analysis.  
328 The results of multivariate analysis of morphometric parameters, bMIPI,  
329 and non-bMIPI clinicopathologic parameters for overall survival are listed in  
330 Table 6. Only low skewness of nuclear irregularity ( $P = 0.020$ ; hazard ratio

331 [HR] = 9.22; 95% CI = 1.42–59.7), high mean of nuclear irregularity ( $P =$   
332 0.047; HR = 5.11; 95% CI = 1.02–25.5), and bMIPI risk group ( $P = 0.025$ ; HR  
333 = 1.80; 95% CI = 1.08–3.01) remained significant adverse prognostic factors.  
334 All other morphometric and clinicopathologic parameters, including  
335 blastoid/pleomorphic morphology, had no more significant influence on  
336 survival in multivariate analysis.

337

### 338 Morphometric Score and Overall Survival

339 We calculated a morphometric score using the two morphometric parameters  
340 with independent adverse prognostic influence in multivariate analysis. One  
341 point was assigned for each of the following risk factors:

- 342 1. Low skewness of nuclear irregularity ( $\leq 3.729$ ).
- 343 2. High mean of nuclear irregularity ( $> 0.1304 \mu\text{m}^2$ ).

344 The morphometric score ranging from 0 to 2 was an adverse prognostic factor  
345 in univariate analysis for overall survival ( $P = 0.0011$ ; HR = 2.34; 95% CI =  
346 1.40–3.90). The survival curves of patients stratified by the morphometric  
347 score are shown in Figure 2J. Multivariate analysis of the morphometric score  
348 and independent clinicopathologic parameters showed that only the  
349 morphometric score ( $P = 0.0028$ ) and B symptoms ( $P = 0.047$ ) were

350 independent adverse prognostic factor (Table 5). Multivariate analysis of the  
351 morphometric score, bMIPI, and non-bMIPI clinicopathologic parameters  
352 showed that only the morphometric score ( $P = 0.0038$ ; HR = 2.32; 95% CI =  
353 1.31–4.11) and bMIPI risk group ( $P = 0.025$ ; HR = 1.66; 95% CI = 1.06–2.58)  
354 remained independent adverse prognostic factors (Table 6).

355

### 356 Visualization of Morphometric Score

357 Density plots were produced to demonstrate the distribution of nuclear  
358 irregularity in each case. Examples of classic MCL, blastoid MCL, and  
359 pleomorphic MCL with different morphometric scores are shown in Figure 4A,  
360 Figure 4B, and Figure 4C, respectively. Higher mean of nuclear irregularity  
361 (right shift of the red vertical line in the density plot) and lower skewness of  
362 nuclear irregularity (less concentration of data at the left in the density plot)  
363 result in a higher morphometric score. With increase of the morphometric  
364 score, there is a trend of increasingly pleomorphic nuclei in the microscopic  
365 images. However, finding an optimal cutoff point of nuclear pleomorphism with  
366 the highest prognostic significance by human eyes is very difficult. The density  
367 plots of nuclear irregularity distribution and microscopic pictures of all cases  
368 can be found in Supplemental Figure S1.

369

370 Correlation of Morphometric Score with Clinicopathologic Features

371 The comparison of clinicopathologic features between cases with a low (0 or

372 1) and high (2) morphometric score is listed in Table 7. A high morphometric

373 score was significantly associated with blastoid/pleomorphic morphology ( $P =$

374 0.0012), Ki-67  $\geq 30\%$  ( $P = 0.0025$ ), and high bMIPI risk group ( $P = 0.0079$ ). Of

375 note, all 26 cases with blastoid or pleomorphic morphology had a high

376 morphometric score of 2 (Figure 4D).

377

378 Morphometric bMIPI Score and Overall Survival

379 Since the morphometric score and bMIPI risk group were independent

380 adverse prognostic factors in multivariate analysis, we calculated a

381 morphometric bMIPI score by adding the morphometric score with a bMIPI

382 score (low risk: 0, intermediate risk: 1, high risk: 2). The morphometric bMIPI

383 score ranging from 0 to 4 was useful for risk stratification of MCL patients, with

384 a  $P$ -value of 0.000009 (Figure 2K). Alternatively, a three-tiered risk grouping

385 (low: 0–1, intermediate: 2–3, high: 4) achieved a  $P$ -value of 0.000001 (Figure

386 2L).

387

388 **Discussion**

389 Blastoid/pleomorphic morphology has long been known to correlate with  
390 worse prognosis in MCL patients.<sup>18</sup> However, identification of these  
391 morphologic variants could be challenging for general pathologists with less  
392 experience.<sup>19</sup> In a recent study, there was only a moderate concordance  
393 (kappa = 0.57) in identification of blastoid/pleomorphic morphology in MCL  
394 among eight reference pathology laboratories of the European MCL  
395 Network,<sup>20</sup> indicating the difficulty even for expert hematopathologists.

396       Theoretically, similar to our previous studies,<sup>21, 22</sup> a direct end-to-end  
397 training process could be used to establish a deep learning model to identify  
398 aggressive morphologic variants of MCL. However, since MCL is a rare type  
399 of B cell lymphoma<sup>1</sup> and its blastoid and pleomorphic variants are even rarer,  
400 it is very difficult to collect numerous cases of each variant for such end-to-  
401 end training. Recently, it has been shown that morphometric parameters can  
402 be used to classify primary intestinal T-cell lymphoma.<sup>23</sup> Here, we analyzed  
403 the disease prognosis based on objective morphometric parameters extracted  
404 from tens of thousands of nuclei among 103 MCL patients to derive a  
405 significant and human-interpretable result.

406       Morphometric studies require accurate contouring of targets. High-quality

407 segmentation of nuclei is essential for correct measurement of nuclear  
408 attributes. Previously, nuclear segmentation was performed using classical  
409 image segmentation methods, such as thresholding, region-based  
410 approaches, energy minimization techniques, and classification-based  
411 segmentation.<sup>24</sup> However, these traditional methods often assume a certain  
412 image pattern of nuclei and are prone to failure when the assumption is  
413 violated. Recently, deep learning has been successful in detection,<sup>21, 22</sup>  
414 classification,<sup>25, 26</sup> and grading<sup>27, 28</sup> of tumors in pathology images. Nowadays,  
415 the best performing nuclear segmentation methods are all deep learning-  
416 based, and their performance is comparable to that of human annotators.<sup>29</sup>  
417 Indeed, our deep learning-based nuclear segmentation model achieved high  
418 performance, thus enabling accurate morphometry (Figure 3; Supplemental  
419 Figure S1). The average aggregated Jaccard index of our predicted nuclei  
420 ranged from 0.685 to 0.696 in different morphologic subtypes, similar to that  
421 of a previously reported best preforming deep learning-based nuclear  
422 segmentation model (average aggregated Jaccard index = 0.691).<sup>29</sup>  
423 More than three decades ago, morphometric studies demonstrated that  
424 lymphoid cells in different areas of normal lymphoid tissue had different  
425 nuclear parameters.<sup>30, 31</sup> Other old studies investigated the nuclear

426 morphometry of non-Hodgkin lymphoma and its potential use in  
427 subclassification.<sup>32-34</sup> Later on, a study showed that the nuclear area of MCL  
428 tumor cells was significantly larger than that of mantle zone lymphocytes in  
429 reactive tonsils.<sup>35</sup> No cases with blastoid/pleomorphic morphology were  
430 included in that study, and their mean nuclear area of MCL measured with  
431 manual annotation by three pathologists was 37.9  $\mu\text{m}^2$ , 37.9  $\mu\text{m}^2$ , and 38.2  
432  $\mu\text{m}^2$ , respectively.<sup>35</sup> Their result was similar to that of our classic MCL (42.42  
433  $\mu\text{m}^2$ ). However, no other morphometric parameters were analyzed in that  
434 study, and correlation with survival was not investigated.<sup>35</sup>

435 Compared to classic MCL, we found that 16 and 13 morphometric  
436 parameters related to nuclear size and shape were significantly different in  
437 blastoid and pleomorphic MCL, respectively (Table 3). Both aggressive  
438 variants had higher mean, higher variance, lower skewness, and/or lower  
439 kurtosis of nuclear length, width, perimeter, area, and/or irregularity. Higher  
440 mean and variance of these morphometric attributes indicates larger and  
441 more irregular nuclei with more variation in size and shape. Lower skewness  
442 reflects less concentration of data at the left in the density plot, whereas lower  
443 kurtosis correlates with more data in shoulders other than the peak or tails in  
444 distribution.<sup>36</sup> Both lower skewness and lower kurtosis of morphometric

445 attributes also contribute to the increased pleomorphism perceived by human  
446 eyes.

447 Theoretically, the more dispersed chromatin in blastoid or pleomorphic  
448 MCL should correlate with higher pixel randomness, namely higher entropy.

449 However, no significant difference in entropy was found between these  
450 aggressive variants and classic MCL (Table 3). Blastoid and pleomorphic  
451 variants are known to have more prominent nucleoli, which result in local  
452 aggregation of pixels and decrease of pixel randomness. This could explain  
453 the lack of significant difference in nuclear entropy between classic MCL and  
454 blastoid or pleomorphic MCL.

455 Using univariate analysis, 16 of the 32 morphometric parameters related  
456 to nuclear size and shape had significant influence on survival (Table 4). Of  
457 note, 14 (87.5%) of them were significantly different between classic MCL and  
458 blastoid or pleomorphic MCL (Table 3). Similar to the difference observed in  
459 blastoid and pleomorphic variants of MCL compared to classic MCL, higher  
460 mean, higher variance, lower skewness, and lower kurtosis of these  
461 morphometric attributes were associated with poor prognosis. Our results  
462 suggest that morphometry could objectively quantify pleomorphism with  
463 prognostic significance.

464 To better evaluate the robustness of the results mentioned above, a  
465 bootstrapping (with 1000 repetitions) procedure was performed for prognostic  
466 analysis of each morphometric parameter. All 16 morphometric parameters  
467 remained prognostically significant after our bootstrap simulation,  
468 demonstrating the robustness of their prognostic effect.

469 Using multivariate analysis, we selected two morphometric parameters  
470 with independent prognostic value (mean and skewness of nuclear  
471 irregularity; Table 5 and Table 6) to calculate a morphometric score. Although  
472 a high morphometric score was strongly associated with blastoid/pleomorphic  
473 morphology ( $P = 0.0012$ ; Table 7), the morphometric score but not  
474 blastoid/pleomorphic morphology had independent prognostic value in  
475 multivariate analysis (Table 5 and Table 6). In fact, a high morphometric score  
476 of 2 identified not only all 26 blastoid/pleomorphic cases but also 53 cases  
477 (68.8%) of classic MCL with worse prognosis (Figure 4D and Figure 2J). In  
478 addition, a low morphometric score of 0 identified 9 cases (11.7%) of classic  
479 MCL with good prognosis (Figure 4D and Figure 2J). Our morphometric  
480 method not only objectively quantified the pleomorphism of tumor cell nuclei  
481 but also revealed a better cutoff value of pleomorphism with higher prognostic  
482 significance than the blastoid/pleomorphic morphology identified by human

483 eyes.

484 Interestingly, a previous morphometric study on follicular lymphoma  
485 showed higher mean, higher standard deviation (square root of variance),  
486 lower skewness, and lower kurtosis of nuclear area in cases composed of  
487 large cells compared to those composed of small cleaved cells.<sup>37</sup> Their finding  
488 suggests a correlation between these morphometric differences and high  
489 tumor grade in follicular lymphoma. It bears some resemblance to our finding  
490 that high mean, high variance, low skewness, and low kurtosis of nuclear size  
491 and irregularity are associated with poor prognosis in MCL. Future study is  
492 needed to clarify whether such phenomenon exists in other types of malignant  
493 lymphoma.

494 Although blastoid/pleomorphic morphology is associated with poor  
495 prognosis in MCL, it has been shown that its prognostic significance is  
496 overruled by the proliferation index Ki-67 in multivariate analysis.<sup>10</sup> Unlike  
497 blastoid/pleomorphic morphology which is identified by human eyes, our  
498 morphometric parameters can be objectively measured. In addition, the  
499 prognostic value of our morphometric score overrode blastoid/pleomorphic  
500 morphology in multivariate analysis. Combining the morphometric score and  
501 bMIPI risk group, our morphometric bMIPI score performed well in risk

502 stratification of MCL patients ( $P = 0.000001$ ), better than bMIPI ( $P = 0.00016$ )  
503 and MIPI ( $P = 0.00099$ ) (Figure 2).

504 In conclusion, we discovered a new independent prognostic factor in MCL  
505 using deep learning-based nuclear morphometry. Such a morphometric score  
506 can be objectively measured, and its prognostic value is more robust than that  
507 of blastoid/pleomorphic morphology. Future large-scale prospective studies  
508 would be helpful to confirm our results.

509

510 **References**

- 511 1. Swerdlow SH, Campo E, Seto M, Müller-Hermelink HK: Mantle cell  
 512 lymphoma. WHO Classification of the Tumours of Haematopoietic and  
 513 Lymphoid Tissues. Edited by Swerdlow SH, Campo E, Harris NL, Jaffe  
 514 ES, Pileri SA, Stein H, Thiele J. Revised 4th ed. Lyon: IARC, 2017. pp.  
 515 285-90
- 516 2. Fu K, Weisenburger DD, Greiner TC, Dave S, Wright G, Rosenwald A,  
 517 Chiorazzi M, Iqbal J, Gesk S, Siebert R, De Jong D, Jaffe ES, Wilson  
 518 WH, Delabie J, Ott G, Dave BJ, Sanger WG, Smith LM, Rimsza L,  
 519 Braziel RM, Muller-Hermelink HK, Campo E, Gascoyne RD, Staudt LM,  
 520 Chan WC, Lymphoma/Leukemia Molecular Profiling P: Cyclin D1-  
 521 negative mantle cell lymphoma: a clinicopathologic study based on  
 522 gene expression profiling. Blood 2005, 106:4315-21
- 523 3. Martin-Garcia D, Navarro A, Valdes-Mas R, Clot G, Gutierrez-Abril J,  
 524 Prieto M, Ribera-Cortada I, Woroniecka R, Rymkiewicz G, Bens S, de  
 525 Leval L, Rosenwald A, Ferry JA, Hsi ED, Fu K, Delabie J,  
 526 Weisenburger D, de Jong D, Climent F, O'Connor SJ, Swerdlow SH,  
 527 Torrents D, Beltran S, Espinet B, Gonzalez-Farre B, Veloza L, Costa D,  
 528 Matutes E, Siebert R, Ott G, Quintanilla-Martinez L, Jaffe ES, Lopez-

- 529                   Otin C, Salaverria I, Puente XS, Campo E, Bea S: CCND2 and CCND3  
530                   hijack immunoglobulin light-chain enhancers in cyclin D1(-) mantle cell  
531                   lymphoma. Blood 2019, 133:940-51
- 532     4.           Chuang WY, Chang H, Chang GJ, Wang TH, Chang YS, Wang TH, Yeh  
533                   CJ, Ueng SH, Chien HP, Chang CY, Wan YL, Hsueh C: Pleomorphic  
534                   mantle cell lymphoma morphologically mimicking diffuse large B cell  
535                   lymphoma: common cyclin D1 negativity and a simple  
536                   immunohistochemical algorithm to avoid the diagnostic pitfall.  
537                   Histopathology 2017, 70:986-99
- 538     5.           Chuang WY, Chang ST, Yuan CT, Chang GJ, Chang H, Yeh CJ, Ueng  
539                   SH, Kao HW, Wang TH, Wan YL, Shih LY, Chuang SS, Hsueh C:  
540                   Identification of CD5/Cyclin D1 Double-negative Pleomorphic Mantle  
541                   Cell Lymphoma: A Clinicopathologic, Genetic, and Gene Expression  
542                   Study. Am J Surg Pathol 2020, 44:232-40
- 543     6.           Mozos A, Royo C, Hartmann E, De Jong D, Baro C, Valera A, Fu K,  
544                   Weisenburger DD, Delabie J, Chuang SS, Jaffe ES, Ruiz-Marcellan C,  
545                   Dave S, Rimsza L, Braziel R, Gascoyne RD, Sole F, Lopez-Guillermo  
546                   A, Colomer D, Staudt LM, Rosenwald A, Ott G, Jares P, Campo E:  
547                   SOX11 expression is highly specific for mantle cell lymphoma and

- 548 identifies the cyclin D1-negative subtype. Haematologica 2009,  
549 94:1555-62
- 550 7. Zeng W, Fu K, Quintanilla-Fend L, Lim M, Ondrejka S, Hsi ED: Cyclin  
551 D1-negative blastoid mantle cell lymphoma identified by SOX11  
552 expression. Am J Surg Pathol 2012, 36:214-9
- 553 8. Hoster E, Dreyling M, Klapper W, Gisselbrecht C, van Hoof A, Kluin-  
554 Nelemans HC, Pfreundschuh M, Reiser M, Metzner B, Einsele H, Peter  
555 N, Jung W, Wormann B, Ludwig WD, Duhrsen U, Eimermacher H,  
556 Wandt H, Hasford J, Hiddemann W, Unterhalt M, German Low Grade  
557 Lymphoma Study G, European Mantle Cell Lymphoma N: A new  
558 prognostic index (MIPI) for patients with advanced-stage mantle cell  
559 lymphoma. Blood 2008, 111:558-65
- 560 9. Royo C, Navarro A, Clot G, Salaverria I, Gine E, Jares P, Colomer D,  
561 Wiestner A, Wilson WH, Vegliante MC, Fernandez V, Hartmann EM,  
562 Trim N, Erber WN, Swerdlow SH, Klapper W, Dyer MJ, Vargas-Pabon  
563 M, Ott G, Rosenwald A, Siebert R, Lopez-Guillermo A, Campo E, Bea  
564 S: Non-nodal type of mantle cell lymphoma is a specific biological and  
565 clinical subgroup of the disease. Leukemia 2012, 26:1895-8
- 566 10. Hoster E, Rosenwald A, Berger F, Bernd HW, Hartmann S,

567 Loddenkemper C, Barth TF, Brousse N, Pileri S, Rymkiewicz G, Kodet  
568 R, Stilgenbauer S, Forstpointner R, Thieblemont C, Hallek M, Coiffier  
569 B, Vehling-Kaiser U, Bouabdallah R, Kanz L, Pfreundschuh M, Schmidt  
570 C, Ribrag V, Hiddemann W, Unterhalt M, Kluin-Nelemans JC, Hermine  
571 O, Dreyling MH, Klapper W: Prognostic Value of Ki-67 Index, Cytology,  
572 and Growth Pattern in Mantle-Cell Lymphoma: Results From  
573 Randomized Trials of the European Mantle Cell Lymphoma Network. J  
574 Clin Oncol 2016, 34:1386-94

575 11. Cheson BD, Fisher RI, Barrington SF, Cavalli F, Schwartz LH, Zucca E,  
576 Lister TA, Alliance AL, Lymphoma G, Eastern Cooperative Oncology G,  
577 European Mantle Cell Lymphoma C, Italian Lymphoma F, European  
578 Organisation for R, Treatment of Cancer/Dutch Hemato-Oncology G,  
579 Grupo Espanol de Medula O, German High-Grade Lymphoma Study  
580 G, German Hodgkin's Study G, Japanese Lymphorrra Study G,  
581 Lymphoma Study A, Group NCT, Nordic Lymphoma Study G,  
582 Southwest Oncology G, United Kingdom National Cancer Research I:  
583 Recommendations for initial evaluation, staging, and response  
584 assessment of Hodgkin and non-Hodgkin lymphoma: the Lugano  
585 classification. J Clin Oncol 2014, 32:3059-68

- 586 12. Chen K, Wang J, Pang J, Cao Y, Xiong Y, Li X, Sun S: MMDetection:  
587 Open MMLab Detection Toolbox and Benchmark.  
588 <https://arxiv.org/abs/1906.07155>, 2019
- 589 13. Lin TY, Maire M, Belongie S, Bourdev L, Girshick R, Hays J, Perona P:  
590 Microsoft COCO: Common Objects in Context.  
591 <https://arxiv.org/abs/1405.0312>, 2014
- 592 14. Chen K, Pang J, Wang J, Xiong Y, Li X, Sun S, Feng W, Liu Z, Shi J,  
593 Ouyang W, Loy CC, Lin D: Hybrid Task Cascade for Instance  
594 Segmentation. 2019 IEEE/CVF Conference on Computer Vision and  
595 Pattern Recognition (CVPR), 2019. pp. 4969-78
- 596 15. He K, Zhang X, Ren S, Sun J: Deep Residual Learning for Image  
597 Recognition. 2016 IEEE Conference on Computer Vision and Pattern  
598 Recognition (CVPR), 2016. pp. 770-8
- 599 16. Shorten C, Khoshgoftaar TM: A survey on Image Data Augmentation  
600 for Deep Learning. J Big Data 2019, 6:60
- 601 17. Ogluszka M, Orzechowska M, Jedroszka D, Witas P, Bednarek AK:  
602 Evaluate Cutpoints: Adaptable continuous data distribution system for  
603 determining survival in Kaplan-Meier estimator. Comput Methods  
604 Programs Biomed 2019, 177:133-9

- 605 18. Bernard M, Gressin R, Lefrere F, Drenou B, Branger B, Caulet-
- 606 Maugendre S, Tass P, Brousse N, Valensi F, Milpied N, Voilat L,
- 607 Sadoun A, Ghandour C, Hunault M, Leloup R, Mannone L, Hermine O,
- 608 Lamy T: Blastic variant of mantle cell lymphoma: a rare but highly  
609 aggressive subtype. Leukemia 2001, 15:1785-91
- 610 19. Dreyling M, Klapper W, Rule S: Blastoid and pleomorphic mantle cell  
611 lymphoma: still a diagnostic and therapeutic challenge! Blood 2018,  
612 132:2722-9
- 613 20. Croci GA, Hoster E, Bea S, Clot G, Enjuanes A, Scott DW, Cabecadas  
614 J, Veloza L, Campo E, Clasen-Linde E, Goswami RS, Helgeland L,  
615 Pileri S, Rymkiewicz G, Reinke S, Dreyling M, Klapper W:  
616 Reproducibility of histologic prognostic parameters for mantle cell  
617 lymphoma: cytology, Ki67, p53 and SOX11. Virchows Arch 2020,  
618 477:259-67
- 619 21. Chuang WY, Chang SH, Yu WH, Yang CK, Yeh CJ, Ueng SH, Liu YJ,  
620 Chen TD, Chen KH, Hsieh YY, Hsia Y, Wang TH, Hsueh C, Kuo CF,  
621 Yeh CY: Successful Identification of Nasopharyngeal Carcinoma in  
622 Nasopharyngeal Biopsies Using Deep Learning. Cancers 2020, 12:507
- 623 22. Chuang WY, Chen CC, Yu WH, Yeh CJ, Chang SH, Ueng SH, Wang

- 624 TH, Hsueh C, Kuo CF, Yeh CY: Identification of nodal micrometastasis  
625 in colorectal cancer using deep learning on annotation-free whole-slide  
626 images. *Mod Pathol* 2021, 34:1901-11
- 627 23. Yu WH, Li CH, Wang RC, Yeh CY, Chuang SS: Machine Learning  
628 Based on Morphological Features Enables Classification of Primary  
629 Intestinal T-Cell Lymphomas. *Cancers* 2021, 13:5463
- 630 24. Vahadane A, Sethi A: Towards generalized nuclear segmentation in  
631 histological images. 13th IEEE International Conference on  
632 BioInformatics and BioEngineering (BIBE). Chania, Greece, 2013. pp.  
633 1-4
- 634 25. Chen CL, Chen CC, Yu WH, Chen SH, Chang YC, Hsu TI, Hsiao M,  
635 Yeh CY, Chen CY: An annotation-free whole-slide training approach to  
636 pathological classification of lung cancer types using deep learning.  
637 *Nat Commun* 2021, 12:1193
- 638 26. Steinbuss G, Kriegsmann M, Zgorzelski C, Brobeil A, Goeppert B,  
639 Dietrich S, Mechtersheimer G, Kriegsmann K: Deep Learning for the  
640 Classification of Non-Hodgkin Lymphoma on Histopathological Images.  
641 *Cancers* 2021, 13:2419
- 642 27. Bulten W, Pinckaers H, van Boven H, Vink R, de Bel T, van Ginneken

- 643                   B, van der Laak J, Hulsbergen-van de Kaa C, Litjens G: Automated  
 644                   deep-learning system for Gleason grading of prostate cancer using  
 645                   biopsies: a diagnostic study. Lancet Oncol 2020, 21:233-41
- 646   28. Strom P, Kartasalo K, Olsson H, Solorzano L, Delahunt B, Berney DM,  
 647                   Bostwick DG, Evans AJ, Grignon DJ, Humphrey PA, Iczkowski KA,  
 648                   Kench JG, Kristiansen G, van der Kwast TH, Leite KRM, McKenney  
 649                   JK, Oxley J, Pan CC, Samaratunga H, Srigley JR, Takahashi H,  
 650                   Tsuzuki T, Varma M, Zhou M, Lindberg J, Lindskog C, Ruusuvuori P,  
 651                   Wahlby C, Gronberg H, Rantalainen M, Egevad L, Eklund M: Artificial  
 652                   intelligence for diagnosis and grading of prostate cancer in biopsies: a  
 653                   population-based, diagnostic study. Lancet Oncol 2020, 21:222-32
- 654   29. Kumar N, Verma R, Anand D, Zhou Y, Onder OF, Tsougenis E, Chen H,  
 655                   Heng PA, Li J, Hu Z, Wang Y, Koohbanani NA, Jahanifar M, Tajeddin  
 656                   NZ, Gooya A, Rajpoot N, Ren X, Zhou S, Wang Q, Shen D, Yang CK,  
 657                   Weng CH, Yu WH, Yeh CY, Yang S, Xu S, Yeung PH, Sun P, Mahbod  
 658                   A, Schaefer G, Ellinger I, Ecker R, Smedby O, Wang C, Chidester B,  
 659                   Ton TV, Tran MT, Ma J, Do MN, Graham S, Vu QD, Kwak JT, Gunda A,  
 660                   Chunduri R, Hu C, Zhou X, Lotfi D, Safdari R, Kascenas A, O'Neil A,  
 661                   Eschweiler D, Stegmaier J, Cui Y, Yin B, Chen K, Tian X, Gruening P,

- 662 Barth E, Arbel E, Remer I, Ben-Dor A, Sirazitdinova E, Kohl M,
- 663 Braunewell S, Li Y, Xie X, Shen L, Ma J, Baksi KD, Khan MA, Choo J,
- 664 Colomer A, Naranjo V, Pei L, Iftekharuddin KM, Roy K, Bhattacharjee
- 665 D, Pedraza A, Bueno MG, Devanathan S, Radhakrishnan S,
- 666 Koduganty P, Wu Z, Cai G, Liu X, Wang Y, Sethi A: A Multi-Organ
- 667 Nucleus Segmentation Challenge. IEEE Transactions on Medical
- 668 Imaging 2020, 39:1380-91
- 669 30. Dardick I: Morphometry of normal human lymphoid tissues. Nuclear
- 670 invaginations and clefts. Arch Pathol Lab Med 1984, 108:197-201
- 671 31. Dardick I, Dardick AM: Morphometry of normal human lymphoid
- 672 tissues. Nuclear parameters for comparative studies of lymphoma.
- 673 Arch Pathol Lab Med 1984, 108:190-6
- 674 32. Crocker J, Jones EL, Curran RC: A comparative study of nuclear form
- 675 factor, area and diameter in non-Hodgkin's lymphomas and reactive
- 676 lymph nodes. J Clin Pathol 1983, 36:298-302
- 677 33. Gupta S, Gupta R, Singh S, Gupta K, Kudesia M: Nuclear
- 678 morphometry and texture analysis of B-cell non-Hodgkin lymphoma:
- 679 utility in subclassification on cytosmears. Diagn Cytopathol 2010,
- 680 38:94-103

- 681 34. Roy S, Joshi K, Choudhury AR, Varma SC, Banerjee CK: Nuclear  
682 morphometric analysis of non-Hodgkin's lymphoma. Pathology 1989,  
683 21:100-4
- 684 35. Baek T, Huh J, Kwak H, Park M, Lee H: Image analytic study of nuclear  
685 area in mantle cell lymphoma. Korean J Hematol 2010, 45:193-6
- 686 36. Westfall PH: Kurtosis as Peakedness, 1905 - 2014. R.I.P. Am Stat  
687 2014, 68:191-5
- 688 37. Stevens MW, Crowley KS, Fazzalari NL, Woods AE: Use of  
689 morphometry in cytological preparations for diagnosing follicular non-  
690 Hodgkin's lymphomas. J Clin Pathol 1988, 41:370-7
- 691

692 **Figure Legends**

693 **Figure 1** Overview of the study design. MCL, mantle cell lymphoma; ROI,  
 694 region of interest.

695 **Figure 2** Survival curves of patients stratified by clinicopathologic features (**A**  
 696 to **I**), morphometric score (**J**), and morphometric bMIPPI score (**K** and **L**).

697 \*Some cases excluded due to incomplete clinical data.

698 **Figure 3** Learning curves and precision-recall curves of our nuclear detection  
 699 model and examples of automatic nuclear segmentation. The learning curves  
 700 showed gradual decrease of loss and increase of average precision (**A**). The  
 701 model achieved a precision of 0.909 with a recall of 0.835 in the testing set  
 702 (**B**). The mean average precision was 0.837, 0.875, and 0.799 for classic,  
 703 blastoid, and pleomorphic MCL, respectively (**C**). Our model performed well in  
 704 automatic contouring (yellow closed lines) of tumor cell nuclei in classic,  
 705 blastoid, and pleomorphic MCL (**D**).

706 **Figure 4** Examples of cases with different morphometric scores. The  
 707 microscopic images with tumor cell nuclei (yellow closed lines) automatically  
 708 delineated by our model and density plots of nuclear irregularity (median =  
 709 blue dotted vertical line) of cases with classic (**A**), blastoid (**B**), and  
 710 pleomorphic (**C**) morphology. A higher mean (red vertical line) and a lower

711 skewness (less concentration of data at the left in the density plot) resulted in  
712 a higher morphometric score. The nuclei in the microscopic pictures appeared  
713 increasingly pleomorphic with increase of the morphometric score. All cases  
714 of blastoid and pleomorphic MCL had a high morphometric score of 2,  
715 whereas classic MCL cases had a morphometric score of 0, 1, or 2 (**D**).  
716

717 **Table 1** The Details of Cases Used for Training, Validation, and Testing of the  
 718 Nuclear Segmentation Model and for Morphometric Analysis

<b>Data set</b>	<b>Morphologic variant</b>		
	<b>Classic</b>	<b>Blastoid</b>	<b>Pleomorphic</b>
Training set	21 cases	5 cases	4 cases
	21 ROIs	5 ROIs	4 ROIs
	3296 tumor cells	732 tumor cells	438 tumor cells
Validation set	4 cases	1 case	1 case
	4 ROIs	1 ROI	1 ROI
	722 tumor cells	160 tumor cells	106 tumor cells
Testing set	21 cases	5 cases	4 cases
	21 ROIs	5 ROIs	4 ROIs
	3784 tumor cells	671 tumor cells	550 tumor cells
Total cases for morphometric analysis	231 non-tumor cells	79 non-tumor cells	37 non-tumor cells
	77 cases	16 cases	10 cases
	231 ROIs*	48 ROIs*	30 ROIs*

719 ROI, region of interest.

720 \*All three ROIs of each case were used for morphometric analysis.

721

722 **Table 2** Clinicopathologic Features and Their Influence on Overall Survival by

723 Univariate Analysis

<b>Parameter</b>	<b>Number</b>	<b>HR (95% CI)</b>	<b>P-value</b>
	(percentage)		
<b>Age at diagnosis (years)</b>			
Range 33–96 (median 64)			
≤ 60	39 (37.9%)	1	
> 60	64 (62.1%)	2.29 (1.33–3.92)	<b>0.0026</b>
<b>Sex</b>			
Female	17 (16.5%)	1	
Male	86 (83.5%)	1.60 (0.77–3.36)	0.21
<b>Stage*</b>			
I or II	11 (11.2%)	1	
III or IV	87 (88.8%)	3.03 (1.21–7.59)	<b>0.018</b>
<b>B symptoms*</b>			
No	66 (76.7%)	1	
Yes	20 (23.3%)	2.21 (1.20–4.07)	<b>0.011</b>
<b>Serum LDH*</b>			
Normal	52 (55.3%)	1	

Elevated	42 (44.7%)	2.00 (1.20–3.34)	<b>0.0079</b>
<b>ECOG score*</b>			
0 or 1	73 (81.1%)	1	
>1	17 (18.9%)	2.00 (1.07–3.74)	<b>0.030</b>
<b>Extranodal site*</b>			
0 or 1	34 (37.0%)	1	
>1	58 (63.0%)	1.05 (0.63–1.76)	0.86
<b>BM/PB involvement*</b>			
No	33 (37.9%)	1	
Yes	54 (62.1%)	1.41 (0.82–2.42)	0.21
<b>MIPI risk group*</b>			
Low	27 (31.0%)		
Intermediate	20 (23.0%)	1.79 (1.30–2.48)	<b>0.00037</b>
High	40 (46.0%)		
<b>Morphologic variant</b>			
Classic	77 (74.8%)	1	
Blastoid/pleomorphic	26 (25.2%)	2.06 (1.20–3.53)	<b>0.0085</b>
<b>Cyclin D1</b>			
Negative	6 (5.8%)	1	

Positive	97 (94.2%)	0.51 (0.18–1.42)	0.20
<b>Ki-67</b>			
< 30%	63 (61.2%)	1	
≥ 30%	40 (38.8%)	1.99 (1.21–3.29)	<b>0.0070</b>
<b>bMIPPI risk group*</b>			
Low	17 (19.6%)		
Intermediate	25 (28.7%)	2.15 (1.46–3.16)	<b>0.000099</b>
High	45 (51.7%)		

724 bMIPPI, biologic mantle cell lymphoma international prognostic index; BM/PB,

725 bone marrow/peripheral blood; CI, confidence interval; ECOG, Eastern

726 Cooperative Oncology Group; HR, hazard ratio; LDH, lactate dehydrogenase;

727 MIPI, mantle cell lymphoma international prognostic index.

728 \*Some cases excluded due to incomplete clinical data.

729 *P*-values < 0.05 shown in boldface.

730

731 **Table 3** Comparison of nuclear morphometric parameters between classic  
 732 and blastoid or pleomorphic mantle cell lymphoma

Nuclear morphometric parameter	Classic MCL (n=77)	Blastoid MCL (n=16)	P-value (blastoid vs. classic MCL)	Pleomorphic MCL (pleomorphic vs. classic MCL)	
<b>Length</b>					
Mean ( $\mu\text{m}$ )	$8.194 \pm 0.834$	$8.967 \pm 0.637$	<b>0.000073</b>	$9.496 \pm 0.575$	<b>0.000007</b>
Variance ( $\mu\text{m}^2$ )	$2.031 \pm 0.696$	$3.012 \pm 0.870$	<b>0.000004</b>	$3.794 \pm 0.958$	<b>&lt; 0.000001</b>
Skewness	$0.632 \pm 0.328$	$0.320 \pm 0.213$	<b>0.000037</b>	$0.419 \pm 0.331$	0.056
Kurtosis	$4.059 \pm 1.043$	$3.122 \pm 0.502$	<b>0.000002</b>	$3.377 \pm 0.687$	<b>0.048</b>
<b>Width</b>					
Mean ( $\mu\text{m}$ )	$6.401 \pm 0.660$	$6.946 \pm 0.495$	<b>0.0024</b>	$7.448 \pm 0.521$	<b>0.000006</b>
Variance ( $\mu\text{m}^2$ )	$1.062 \pm 0.522$	$1.720 \pm 0.587$	<b>0.000021</b>	$2.445 \pm 0.729$	<b>&lt; 0.000001</b>
Skewness	$0.285 \pm 0.326$	$0.247 \pm 0.302$	0.67	$0.167 \pm 0.228$	0.27
Kurtosis	$3.902 \pm 0.807$	$3.538 \pm 0.817$	0.11	$3.333 \pm 0.579$	<b>0.034</b>
<b>Perimeter</b>					
Mean ( $\mu\text{m}$ )	$24.17 \pm 2.49$	$26.39 \pm 1.88$	<b>0.0011</b>	$28.10 \pm 1.79$	<b>0.000006</b>
Variance ( $\mu\text{m}^2$ )	$14.62 \pm 6.24$	$23.28 \pm 7.67$	<b>0.000005</b>	$31.34 \pm 8.57$	<b>&lt; 0.000001</b>

Skewness	$0.345 \pm 0.331$	$0.135 \pm 0.242$	<b>0.018</b>	$0.192 \pm 0.253$	0.16
Kurtosis	$3.794 \pm 0.846$	$3.162 \pm 0.534$	<b>0.0052</b>	$3.164 \pm 0.514$	<b>0.024</b>
<b>Area</b>					
Mean ( $\mu\text{m}^2$ )	$42.42 \pm 8.78$	$50.42 \pm 7.25$	<b>0.00097</b>	$57.49 \pm 7.41$	<b>0.000001</b>
Variance ( $\mu\text{m}^4$ )	$181.9 \pm 117.7$	$329.5 \pm 150.8$	<b>0.000037</b>	$514.3 \pm 177.1$	<b>&lt; 0.000001</b>
Skewness	$0.761 \pm 0.358$	$0.633 \pm 0.309$	0.19	$0.720 \pm 0.241$	0.73
Kurtosis	$4.694 \pm 1.516$	$3.933 \pm 1.202$	0.063	$3.903 \pm 0.815$	0.11
<b>Length/width ratio</b>					
Mean	$1.291 \pm 0.032$	$1.304 \pm 0.027$	0.14	$1.293 \pm 0.362$	0.88
Variance	$0.038 \pm 0.008$	$0.040 \pm 0.006$	0.26	$0.043 \pm 0.015$	0.30
Skewness	$1.389 \pm 0.299$	$1.297 \pm 0.323$	0.27	$1.600 \pm 0.645$	0.33
Kurtosis	$6.108 \pm 2.138$	$5.647 \pm 2.129$	0.43	$7.449 \pm 4.916$	0.42
<b>Circularity</b>					
Mean	$0.760 \pm 0.015$	$0.753 \pm 0.014$	0.096	$0.758 \pm 0.018$	0.70
Variance	$0.008 \pm 0.001$	$0.009 \pm 0.001$	0.083	$0.010 \pm 0.002$	0.067
Skewness	$-0.703 \pm 0.192$	$-0.662 \pm 0.209$	0.45	$-0.864 \pm 0.281$	0.11
Kurtosis	$3.455 \pm 0.502$	$3.324 \pm 0.581$	0.36	$3.792 \pm 0.835$	0.24
<b>Irregularity</b>					
Mean ( $\mu\text{m}^2$ )	$0.161 \pm 0.040$	$0.201 \pm 0.041$	<b>0.00062</b>	$0.216 \pm 0.040$	<b>0.00013</b>

Variance ( $\mu\text{m}^4$ )	$0.031 \pm 0.015$	$0.042 \pm 0.015$	<b>0.0088</b>	$0.052 \pm 0.017$	<b>0.00011</b>
Skewness	$2.960 \pm 0.889$	$2.373 \pm 0.519$	<b>0.013</b>	$2.532 \pm 0.773$	0.15
Kurtosis	$17.34 \pm 12.03$	$11.14 \pm 5.13$	<b>0.047</b>	$12.63 \pm 6.85$	0.23
<b>Entropy</b>					
Mean	$5.758 \pm 0.238$	$5.707 \pm 0.165$	0.42	$5.777 \pm 0.243$	0.82
Variance	$0.082 \pm 0.023$	$0.080 \pm 0.014$	0.62	$0.088 \pm 0.022$	0.42
Skewness	$-0.082 \pm 0.203$	$-0.044 \pm 0.174$	0.49	$-0.043 \pm 0.213$	0.57
Kurtosis	$3.281 \pm 0.588$	$3.270 \pm 0.208$	0.94	$3.128 \pm 0.284$	0.42

733 MCL, mantle cell lymphoma.

734 The values of morphometric parameters were mean  $\pm$  standard deviation.

735 *P*-values  $< 0.05$  shown in boldface.

736

737 **Table 4** Nuclear Morphometric Parameters and Their Influence on Overall

738 Survival by Univariate Analysis

Nuclear morphometric parameter	Cutoff value	HR (95% CI) for value > cutoff	P-value	HR (95% CI) (bootstrapping)	P-value (bootstrapping)
		value		1000 times)	1000 times)
<b>Length</b>					
Mean ( $\mu\text{m}$ )	8.038	1.80 (1.06–3.06)	<b>0.031</b>	1.79 (1.15–2.93)	<b>0.034</b>
Variance ( $\mu\text{m}^2$ )	1.626	2.15 (1.19–3.88)	<b>0.011</b>	2.14 (1.31–3.88)	<b>0.013</b>
Skewness	0.7112	0.50 (0.29–0.87)	<b>0.014</b>	0.49 (0.27–0.81)	<b>0.013</b>
Kurtosis	4.170	0.56 (0.31–1.01)	0.055	0.55 (0.30–1.00)	0.051
<b>Width</b>					
Mean ( $\mu\text{m}$ )	6.211	1.77 (1.05–3.00)	<b>0.032</b>	1.82 (1.13–2.92)	<b>0.027</b>
Variance ( $\mu\text{m}^2$ )	0.7860	1.98 (1.13–3.48)	<b>0.018</b>	2.02 (1.22–3.65)	<b>0.015</b>
Skewness	0.4814	1.31 (0.75–2.27)	0.34	1.34 (0.76–2.36)	0.31
Kurtosis	3.274	0.72 (0.42–1.22)	0.22	0.70 (0.36–1.28)	0.20
<b>Perimeter</b>					
Mean ( $\mu\text{m}$ )	23.41	1.82 (1.07–3.10)	<b>0.027</b>	1.84 (1.15–3.17)	<b>0.026</b>
Variance ( $\mu\text{m}^2$ )	12.07	1.98 (1.14–3.44)	<b>0.015</b>	2.01 (1.22–3.53)	<b>0.014</b>
Skewness	0.5471	0.46 (0.23–0.90)	<b>0.023</b>	0.45 (0.22–0.82)	<b>0.023</b>

Kurtosis	3.857	0.56 (0.33–0.96)	<b>0.036</b>	0.57 (0.31–0.93)	<b>0.043</b>
<b>Area</b>					
Mean ( $\mu\text{m}^2$ )	37.54	1.81 (1.05–3.11)	<b>0.032</b>	1.83 (1.12–3.22)	<b>0.030</b>
Variance ( $\mu\text{m}^4$ )	118.1	2.10 (1.18–3.73)	<b>0.012</b>	2.11 (1.27–3.95)	<b>0.012</b>
Skewness	0.8512	0.65 (0.39–1.08)	0.096	0.64 (0.38–1.04)	0.088
Kurtosis	4.738	0.75 (0.44–1.28)	0.29	0.76 (0.44–1.27)	0.33
<b>Length/width Ratio</b>					
Mean	1.295	1.69 (1.03–2.75)	<b>0.036</b>	1.70 (0.99–2.88)	<b>0.037</b>
Variance	0.03077	1.47 (0.74–2.90)	0.27	1.44 (0.69–3.52)	0.30
Skewness	1.414	0.66 (0.40–1.10)	0.11	0.66 (0.35–1.11)	0.11
Kurtosis	5.211	0.61 (0.37–0.99)	<b>0.045</b>	0.60 (0.35–0.96)	<b>0.045</b>
<b>Circularity</b>					
Mean	0.7686	0.58 (0.32–1.05)	0.073	0.57 (0.28–1.07)	0.070
Variance	0.008286	1.49 (0.92–2.41)	0.11	1.50 (0.90–2.57)	0.10
Skewness	-0.8397	1.42 (0.79–2.53)	0.24	1.44 (0.74–2.88)	0.23
Kurtosis	3.382	0.80 (0.49–1.29)	0.35	0.79 (0.48–1.33)	0.36
<b>Irregularity</b>					
Mean ( $\mu\text{m}^2$ )	0.1304	2.63 (1.34–5.18)	<b>0.0050</b>	2.64 (1.55–4.98)	<b>0.0051</b>
Variance ( $\mu\text{m}^4$ )	0.02746	1.58 (0.96–2.60)	0.073	1.58 (0.99–2.73)	0.076

Skewness	3.729	0.14 (0.03–0.57)	<b>0.0061</b>	0.13 (0.01–0.40)	<b>0.0048</b>
Kurtosis	12.90	0.47 (0.28–0.77)	<b>0.0029</b>	0.45 (0.25–0.77)	<b>0.0024</b>
<b>Entropy</b>					
Mean	5.913	0.75 (0.41–1.38)	0.35	0.75 (0.33–1.45)	0.37
Variance	0.06866	1.34 (0.78–2.31)	0.29	1.38 (0.77–2.64)	0.25
Skewness	0.1978	0.38 (0.12–1.21)	0.10	0.37 (0.01–0.84)	0.090
Kurtosis	3.188	0.65 (0.40–1.07)	0.088	0.65 (0.39–1.03)	0.091

739 CI, confidence interval; HR, hazard ratio.

740 *P*-values < 0.05 shown in boldface.

741

742

743 **Table 5** Influence of Morphometric Parameters (or the Morphometric Score)

744 and Independent Clinicopathologic Parameters on Overall Survival by

745 Multivariate Analysis

<b>Parameter</b>	<b>Hazard ratio (95% CI)</b>	<b>P-value</b>
Morphometric parameters and independent clinicopathologic parameters		
Low skewness of nuclear irregularity	12.7 (2.13–76.5)	<b>0.0054</b>
High mean of nuclear irregularity	5.90 (1.16–30.1)	<b>0.033</b>
High mean of nuclear width		0.056
High variance of nuclear length		0.058
High variance of nuclear perimeter		0.15
High mean of nuclear length		0.20
Low skewness of nuclear perimeter		0.37
Low skewness of nuclear length		0.53
Low kurtosis of nuclear length/width ratio		0.55
High mean of nuclear length/width ratio		0.69
High variance of nuclear area		0.86
Low kurtosis of nuclear irregularity		0.88
High mean of nuclear perimeter		0.88

Low kurtosis of nuclear perimeter		0.88
High variance of nuclear width		0.90
High mean of nuclear area		0.91
Age > 60 Years	3.14 (1.15–8.54)	<b>0.025</b>
Elevated serum LDH	2.02 (0.95–4.30)	0.070
Stage III or IV	2.64 (0.76–9.21)	0.13
B symptoms	1.81 (0.77–4.27)	0.17
ECOG score > 1	1.78 (0.76–4.19)	0.18
Blastoid/pleomorphic morphology	1.44 (0.55–3.77)	0.46
Ki-67 ≥ 30%	0.88 (0.36–2.18)	0.78
Morphometric score and independent clinicopathologic parameters		
Morphometric score	2.40 (1.35–4.25)	<b>0.0028</b>
Age > 60 years	1.69 (0.81–3.54)	0.17
Stage III or IV	2.31 (0.80–6.64)	0.12
B symptoms	2.07 (1.01–4.22)	<b>0.047</b>
Elevated serum LDH	1.45 (0.77–2.73)	0.26
ECOG score > 1	1.77 (0.82–3.83)	0.15
Blastoid/pleomorphic morphology	1.05 (0.47–2.35)	0.90

Ki-67 ≥ 30%	1.12 (0.54–2.34)	0.75
-------------	------------------	------

---

746 CI, confidence interval; ECOG, Eastern Cooperative Oncology Group; LDH,

747 lactate dehydrogenase.

748 *P*-values < 0.05 shown in boldface.

749

750

751 **Table 6** Influence of Morphometric Parameters (or the Morphometric Score),

752 bMIPI, and Non-bMIPI Clinicopathologic Parameters on Overall Survival by

753 Multivariate Analysis

<b>Parameter</b>	<b>Hazard ratio (95% CI)</b>	<b>P-value</b>
Morphometric parameters, bMIPI, and non-		
bMIPI clinicopathologic parameters		
Low skewness of nuclear irregularity	9.22 (1.42–59.7)	<b>0.020</b>
High mean of nuclear irregularity	5.11 (1.02–25.5)	<b>0.047</b>
High mean of nuclear length		0.15
High variance of nuclear length		0.17
High variance of nuclear perimeter		0.19
High mean of nuclear width		0.28
Low kurtosis of nuclear perimeter		0.41
Low kurtosis of nuclear irregularity		0.60
High mean of nuclear length/width ratio		0.63
Low kurtosis of nuclear length/width ratio		0.78
Low skewness of nuclear length		0.83
High variance of nuclear area		0.86
High mean of nuclear perimeter		0.88

High variance of nuclear width		0.89
High mean of nuclear area		0.90
Low skewness of nuclear perimeter		0.91
bMIPPI risk group	1.80 (1.08–3.01)	<b>0.025</b>
Stage III or IV	3.14 (0.93–10.7)	0.066
B symptoms	1.56 (0.71–3.43)	0.27
Blastoid/pleomorphic morphology	1.25 (0.56–2.79)	0.59
Morphometric score and independent clinicopathologic parameters		
Morphometric score	2.32 (1.31–4.11)	<b>0.0038</b>
bMIPPI risk group	1.66 (1.06–2.58)	<b>0.025</b>
Stage III or IV	2.24 (0.81–6.17)	0.12
B symptoms	1.97 (1.00–3.87)	0.050
Blastoid/pleomorphic morphology	1.07 (0.54–2.12)	0.85

754 bMIPPI, biologic mantle cell lymphoma international prognostic index; CI,

755 confidence interval.

756 *P*-values < 0.05 shown in boldface.

757

758 **Table 7** Comparison of clinicopathologic features between cases with a low  
 759 and high morphometric score

Parameter	Low morphometric score (MS = 0 or 1; n = 24)	High morphometric score (MS = 2; n = 79)	P-value
Age at diagnosis (years)			
≤ 60	13 (54.2%)	26 (32.9%)	
> 60	11 (45.8%)	53 (67.1%)	0.060
Sex			
Female	5 (20.8%)	12 (15.2%)	
Male	19 (79.2%)	67 (84.8%)	0.74
Stage*			
I or II	3 (13.0%)	8 (10.7%)	
III or IV	20 (87.0%)	67 (89.3%)	1.0
B symptoms*			
No	16 (80.0%)	50 (75.8%)	
Yes	4 (20.0%)	16 (24.2%)	0.93
Serum LDH*			
Normal	15 (65.2%)	37 (52.1%)	
Elevated	8 (34.8%)	34 (47.9%)	0.27

## ECOG score\*

0 or 1	21 (91.3%)	52 (77.6%)	
> 1	2 (8.7%)	15 (22.4%)	0.26

## Extranodal site\*

0 or 1	8 (34.8%)	26 (37.7%)	
> 1	15 (65.2%)	43 (62.3%)	0.80

## BM/PB involvement\*

No	7 (30.4%)	26 (40.6%)	
Yes	16 (69.6%)	38 (59.4%)	0.39

## MIP1 risk group\*

Low to intermediate	14 (63.6%)	33 (50.8%)	
High	8 (36.4%)	32 (49.2%)	0.30

## Morphologic variant

Classic	24 (100%)	53 (67.1%)	
Blastoid/pleomorphic	0 (0%)	26 (32.9%)	<b>0.0012</b>

## Cyclin D1

Negative	0 (0%)	6 (7.6%)	
Positive	24 (100%)	73 (92.4%)	0.37

## Ki-67

< 30%	21 (87.5%)	42 (53.2%)	
≥ 30%	3 (12.5%)	37 (46.8%)	<b>0.0025</b>
<b>bMIPI risk group*</b>			
Low to intermediate	16 (72.7%)	26 (40.0%)	
High	6 (27.3%)	39 (60.0%)	<b>0.0079</b>

760 bMIPI, biologic mantle cell lymphoma international prognostic index; BM/PB,

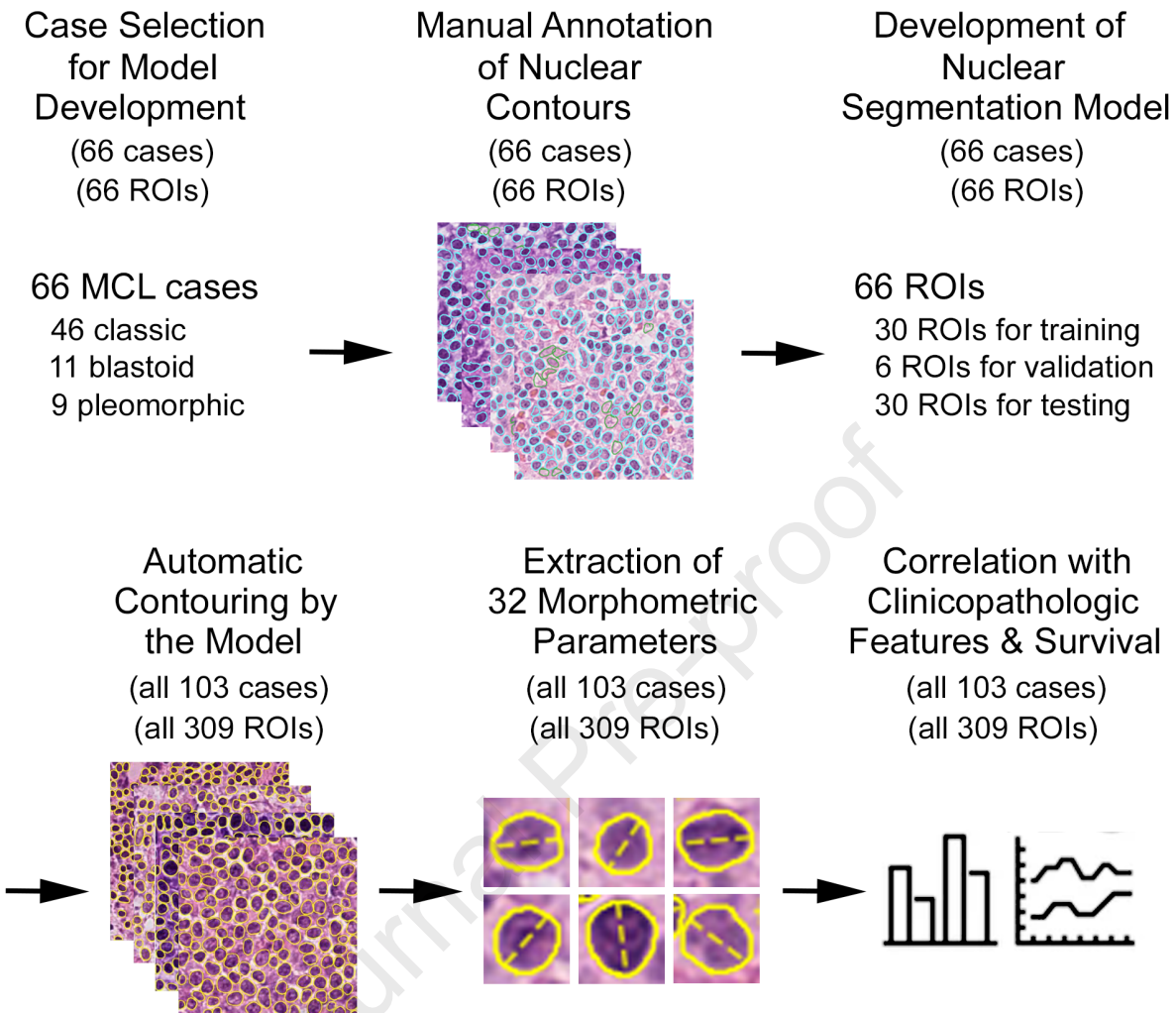
761 bone marrow/peripheral blood; CI, confidence interval; ECOG, Eastern

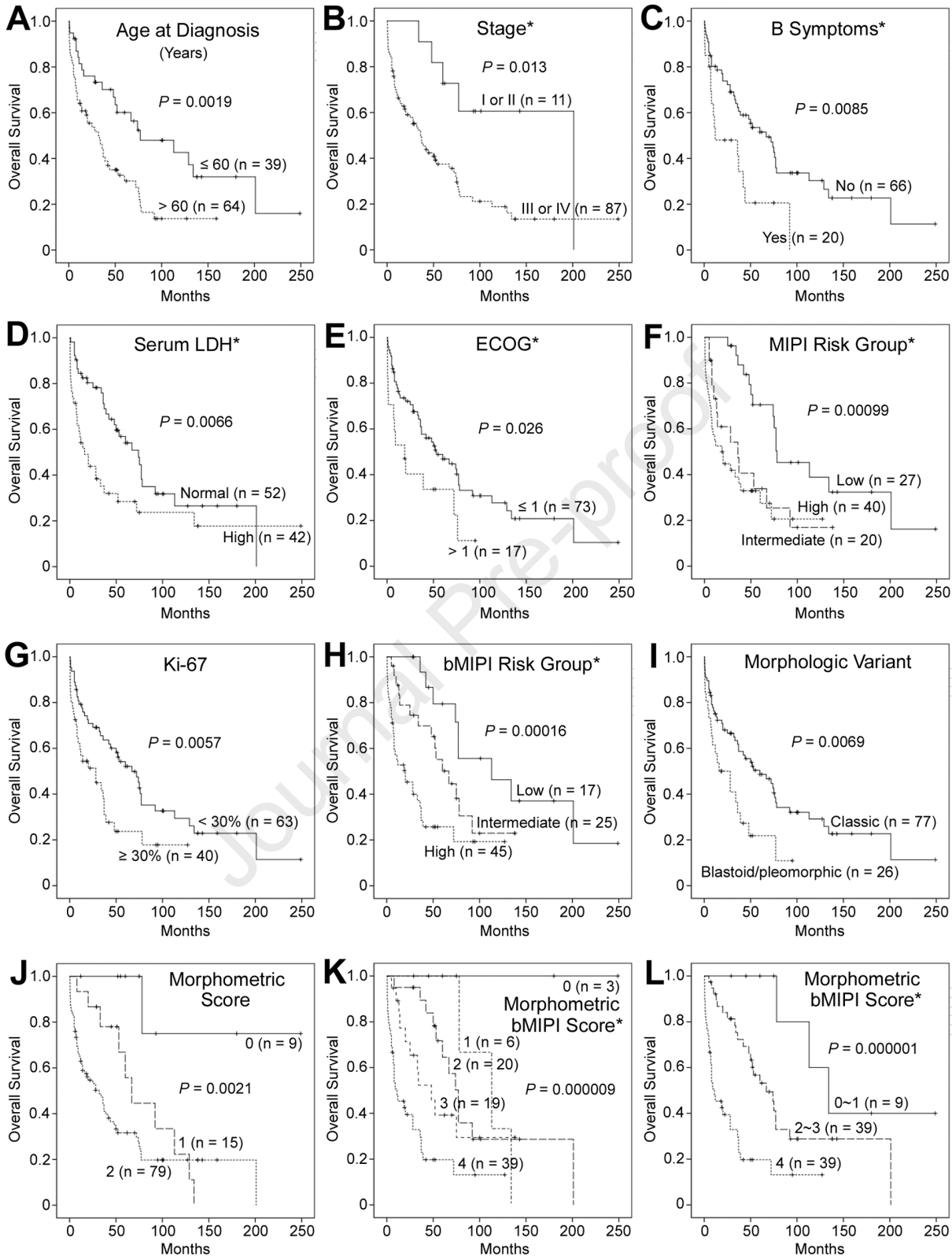
762 Cooperative Oncology Group; LDH, lactate dehydrogenase; MIPI, mantle cell

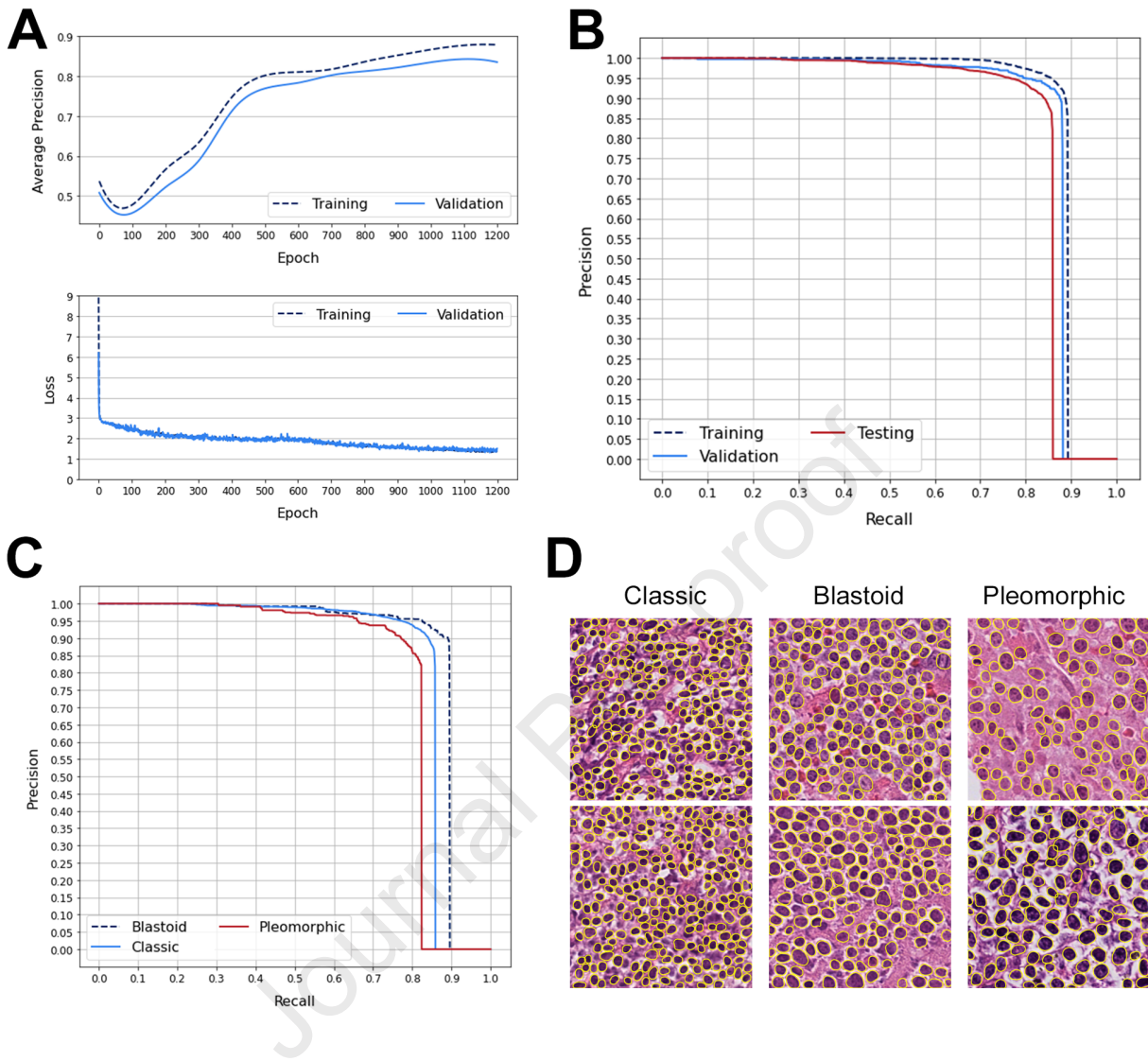
763 lymphoma international prognostic index; MS, morphometric score.

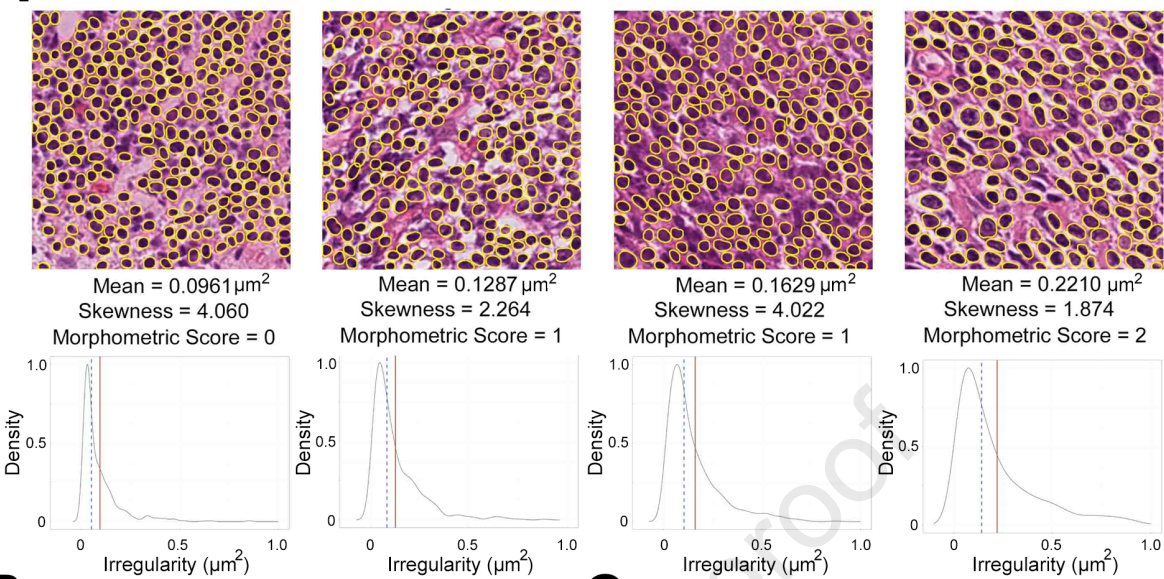
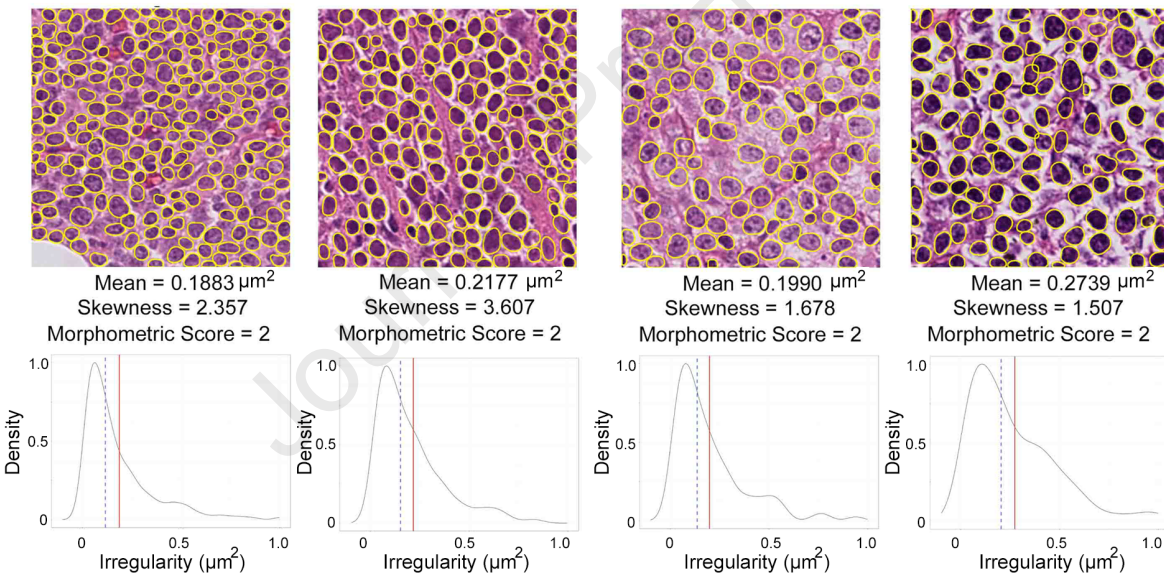
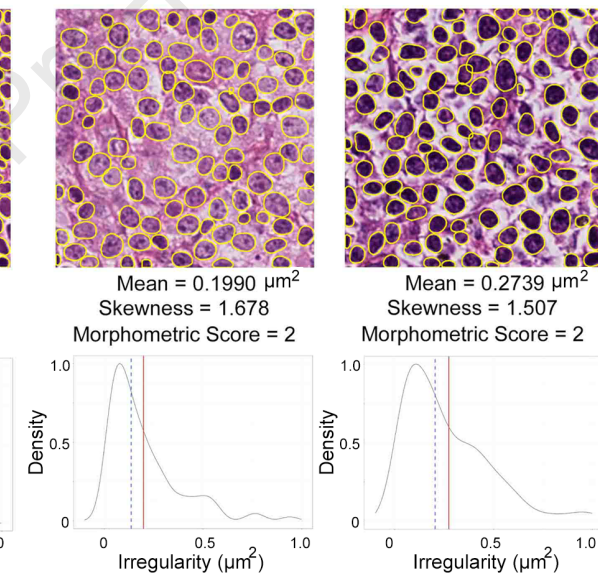
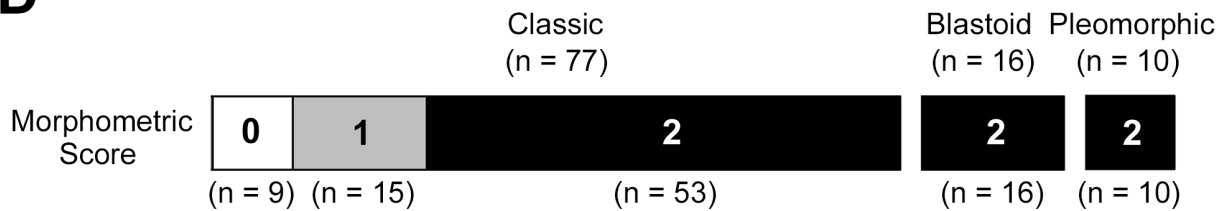
764 \*Some cases excluded due to incomplete clinical data.

765 *P*-values < 0.05 shown in boldface.







**A****B****C****D**

1    **Supplemental Figure Legends**

2    **Supplemental Figure S1** Representative regions of interest and density plots  
3    of nuclear irregularity (mean = red line; median = blue dotted line) of all cases  
4    sorted by morphometric score. The nuclear contours (yellow closed lines) of  
5    tumor cells were automatically delineated by our model.

6    **Supplementary Figure S2** The distribution of each nuclear morphometric  
7    parameter (left) with a cutoff value (vertical line) determined by the software  
8    Evaluate Cutpoints.<sup>17</sup> The survival curves stratified by each morphometric  
9    parameter using the cutoff value are also shown (right). *P*-values less than  
10   0.05 are shown in red.